Electronic Supplementary Material (ESI) for Journal of Materials Chemistry A

Supplementary Information

Self-Assembled Hollow Mesoporous Co_3O_4 Hybrid Architectures: A Facile Synthesis and Application in Li-ion Batteries

Nulu Venugopal, Dong-Ju Lee, Yun Jung Lee*, Yang-Kook Sun *

Department of Energy Engineering, Hanyang University, Seoul 133-791, Republic of Korea

*Corresponding author : yksun@hanyang.ac.kr, yjlee94@hanyang.ac.kr

Mechanistic Investigation of the Reaction

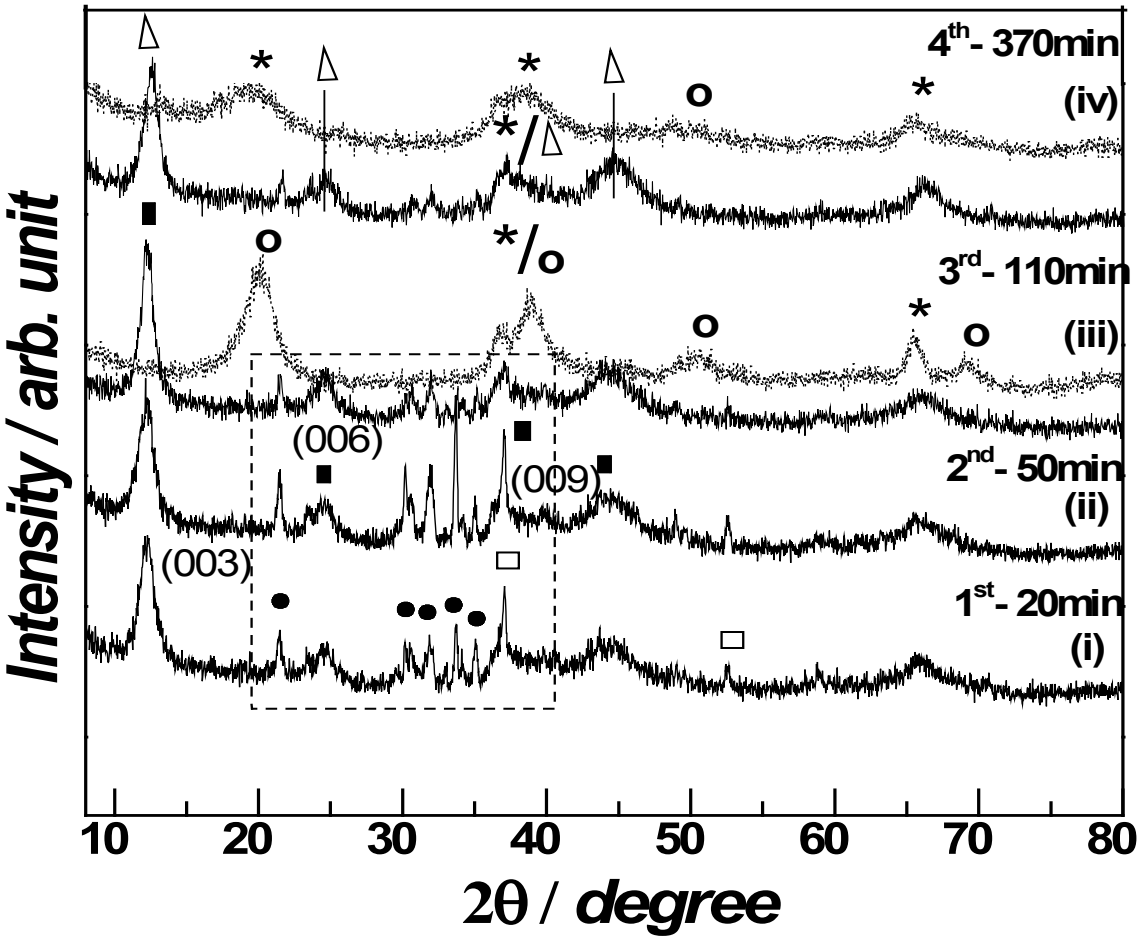

Fig. S1. XRD patterns of the collected precipitates at different stages of the reaction (sample C series): asterisk, Co_3O_4; solid rectangle, HT-type $Co^{II}_{1-x}Co^{III}_{x}(OH)_2$ $(NO_3)x\cdot nH_2O$; open circle, CoO(OH); open triangle, defective HT-type $Co^{II}_{1-x}Co^{III}_{x}(OH)_2$ $(NO_3)x\cdot nH_2O$; solid circle, Li_2O_2 ; open square, $LiNO_3$.

The XRD patterns of the samples collected at different stages during the course of the reaction (decided on the basis of color changes and the amount of precipitates obtained) for C-series are shown in Fig. S1. The first sample (obtained after 20 min, see Fig. S1-i) showed patterns typical of hydrotalcite type $Co^{II}_{1-x}Co^{III}_{x}(OH)_2(NO_3)x\cdot nH_2O$ layered structure (in short, Co(II,III)HTlc) with an interlayer distance of d_{003}=7.33 Å and some portion of unreacted Li_2O_2 (marked by solid circles), together with small and broad peaks of spinel Co_3O_4 (2θ = 66°). We believe that, after the addition of Li_2O_2 (LO), LO slowly reacts with $Co(NO_3)_2\cdot 6H_2O$ (CN) by a general neutralization reaction between mild basic LO and acidic NO_3^- group (obtained from starting precursor, CN). This reaction results in the formation of salt ($LiNO_3$), together with the release of oxygen, which is useful for the oxidation of Co(II) cations, which could lead to the formation of Co(II,III) HTlc phase alongside Co_3O_4. At this stage, some amount of nitrate ions is consumed through the intercalation process that occurs within the HTlc layered structures, whereas the remaining nitrate ions are utilized in the reaction with LO, which further increases the amount of salt ($LiNO_3$) and enhances the oxidative atmosphere as the reaction proceeds. The $LiNO_3$ and other *in-situ* obtained unknown organic precursors are highly soluble in solvent (iso-proponol) and can be separated out easily by centrifugation. This Co_3O_4 phase formation at the early stage of the reaction is in contrast to the reported aqueous methods, which require prolonged reaction times to obtain small amounts of the Co_3O_4 phase.[1-4] The main diffraction patterns of the samples obtained after the second and third stages (Figs. S1-ii and S1-iii) are consistent with the well-known hydrotalcite-like phase, i.e., $d_{003}=2d_{006}=3d_{009}$ with corresponding d values >7 Å (7.28 Å and 7.21 Å, respectively). During prolonged reaction times, LO was consumed slowly to produce oxygen, and this dissolved oxygen gradually oxidized the Co(II,III) HTlc compound to Co_3O_4, which formed a black precipitate (Fig. S1-iv). This

observation is confirmed by the increase in width and height of the peak at 2θ = 66° (corresponding to the Co_3O_4 phase) when moving from stage (i) to (iv) in Fig. S1. The pH values were also recorded before the addition of precipitating agent (LO) to the reaction mixture and 20 min, 50 min, 110 min and 370 min after the addition of LO. The measured values were 3.4 (before LO addition), 4.5 (20 min), 5.1 (50 min), 5.6 (110 min), and 6.9(370 min), respectively. The XRD results for the samples that were washed with water at the third and fourth stages are indicated by dotted line patterns. The formation of a $CoOOH/Co_3O_4$ mixture was observed, with CoOOH being the dominant phase at the third stage, while Co_3O_4 was the predominant phase at the fourth stage (see Figs. S1-iii and S1-iv); this result is consistent with the XRD results discussed in the main text. These phases were further identified in the FTIR investigation shown in Fig. S2. The high-intensity peaks at 3419–3461 $cm^{-1}$and 1625–1657 cm^{-1} were assigned to O-H group stretching of water molecules and hydrogen bound -OH groups.[2,4] The peaks at 1511 cm^{-1}, 1432 cm^{-1}, and 1070 cm^{-1} correspond to the presence of the adsorbed alcohol (isoproponol) molecules of –COO and –C=O on the obtained solid surfaces.[4, 5–7] The sharp bands at around 1380 cm^{-1} and 860 cm^{-1} denote the v_3 and v_2 vibrational modes of intercalated NO_3^- groups with D_{3h} symmetry.[6] We assigned the absorption bands at around 623 cm^{-1} to Co-O-H, and those at 630 cm^{-1} and 511 cm^{-1} to Co-O vibrations.[6,7] In Fig. S2a, the absence of peaks for Co-O suggests the presence of $Co(OH)_2$ phase as the dominant one at the initial stage of the reaction; a split at this region in the fourth stage sample (Fig. S2d) confirms Co_3O_4 phase formation, in agreement with the XRD results.

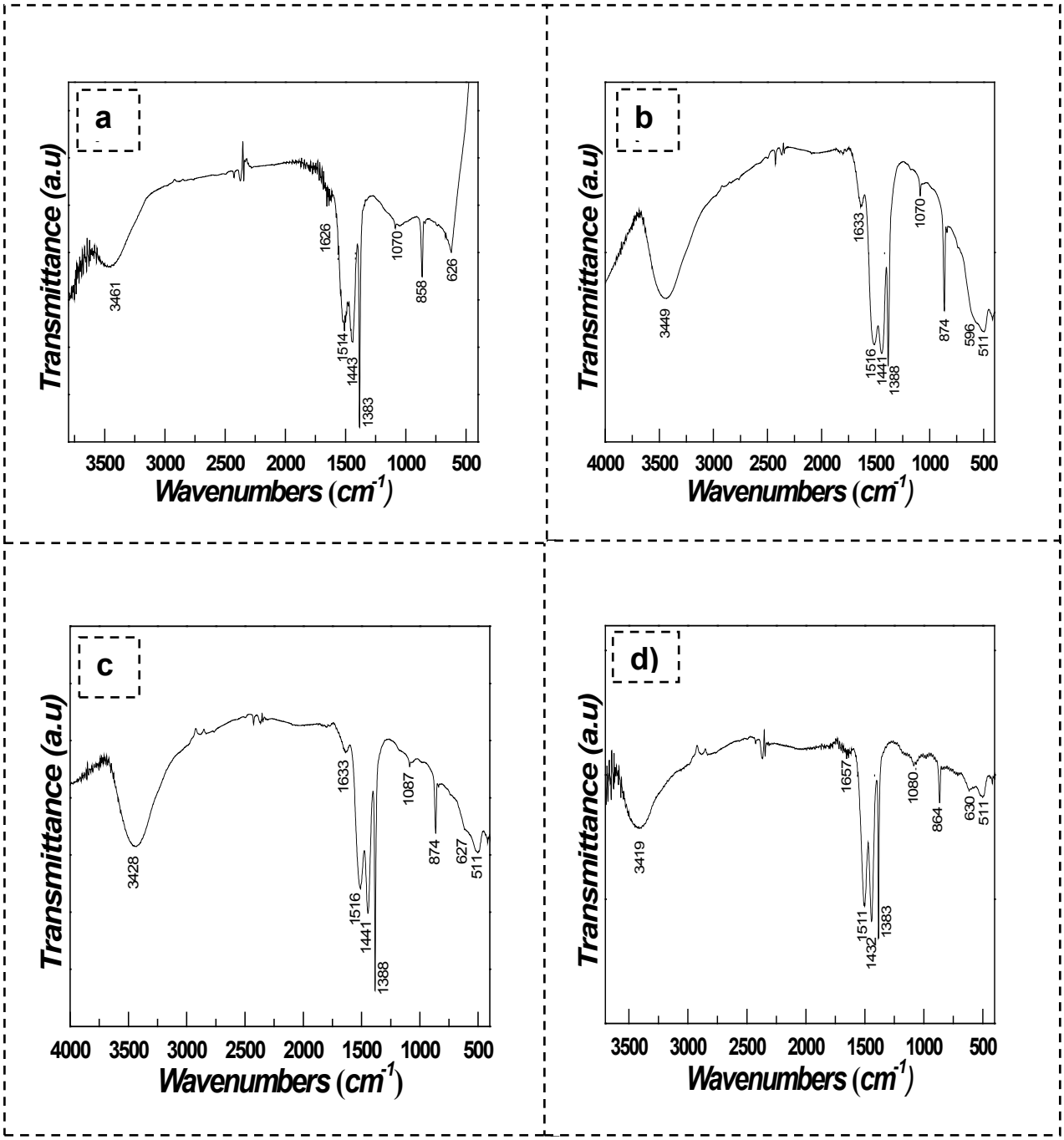

Fig. S2. FTIR spectra of the collected precipitates at different stages of the reaction mixture (C series): (a) first stage (20 min), (b) second stage (50 min), (c) third stage (110 min), and (d) fourth stage (370 min).

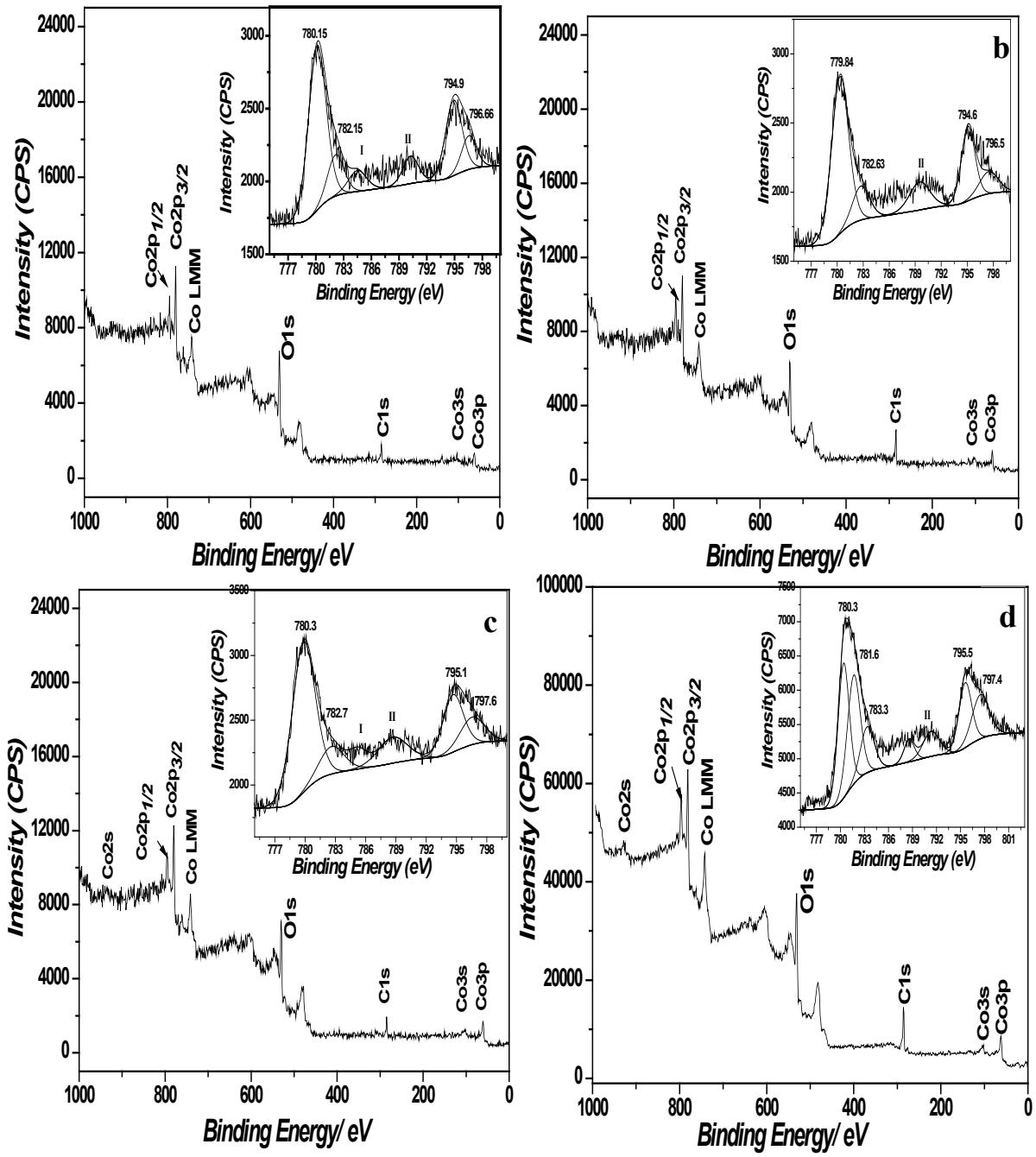

Fig. S3. XPS analysis spectra of samples (a) C3, (b) CC3, (c) C4, and (d) CC4. Inset images are the corresponding high-resolution survey of Co 2p.

Figure S3 shows the complete XPS analysis results for samples C3, C4, CC3, and CC4. The common peak at a binding energy of 286.0 eV is the aliphatic carbon while the other main peaks match well with the Co 2p, O 1s, and C 1s regions. We attributed the increase in intensity of the carbon peak in samples CC3 and CC4 to the presence of CNTs (shown in Figs. S3b and S3d). The high-resolution images of the Co 2p spin orbit components are shown as insets in Fig. S3a-d. In samples C3 and CC3, Co_3O_4 phase is identified by the appearance of spin orbit peaks at 794.9 eV and 794.6 eV for Co $2p_{1/2}$, and 780.15 and 779.84 eV for Co $2p_{3/2}$.[8, 9] Shakeup satellites at about 5 eV from the Co 2p peaks occurred mainly due to the presence of surface hydroxyl groups, but could also have been produced by the Co(III)-OH phase.[10] The appearance of low-intensity shake-up satellite peaks (II) at around 9 eV from the main spin orbit component also indicated dominant Co_3O_4 phase formation,[10] demonstrating that overnight oven drying of the as-prepared samples increased Co_3O_4 phase. The annealed samples (C4 and CC4) had high intensity peaks of Co_3O_4, indicating that the annealing process facilitated the Co_3O_4 phase formation. Further, the marked peaks at ~781.6–783.3 eV and 796.5–797.6 eV observed for all samples indicated a shift in the main spin-orbit peaks caused by chemical interactions between minor amounts of Co(II) and Co(III) ions to the solvent molecules, hydroxyl groups, and carboxylate groups that occur during the process of phase transformation.[10,11] These peaks were very clear in the samples annealed at 200 °C. Further, Co_3O_4 phase is conformed by high resolution O 1s peaks of C4 and CC4 are shown in Fig. S4 (discussed in the main text).

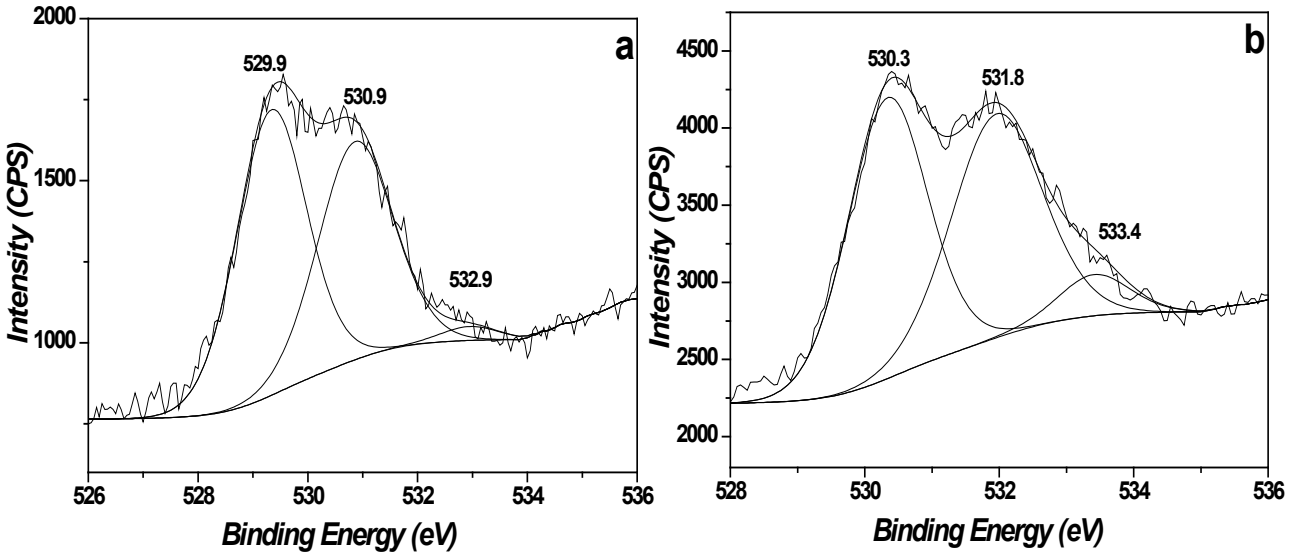

Fig. S4. High resolution XPS analyses O 1s for samples (a) C4 and (b) CC4

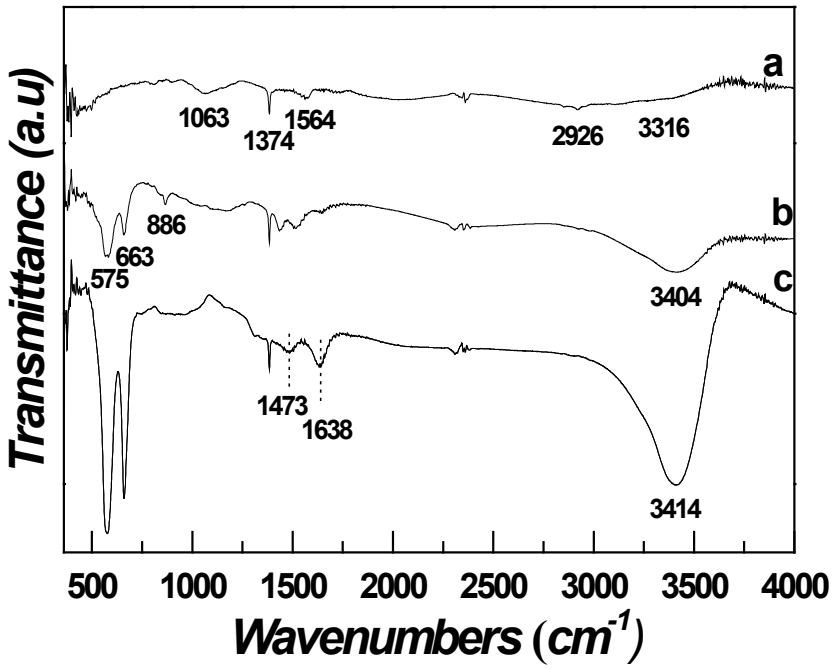

Fig. S5. FTIR spectra of sample (a) fCNT , (b) CC4, and (c) C4

Figure S5 shows the FTIR analysis of the samples fCNT, C4, and CC4 (discussed in main text). After heat treatment, the intensity of the solvent-absorbed molecules (at 1473 cm^{-1}) on the nanoparticulates decreased due to evaporation of organic functional groups.

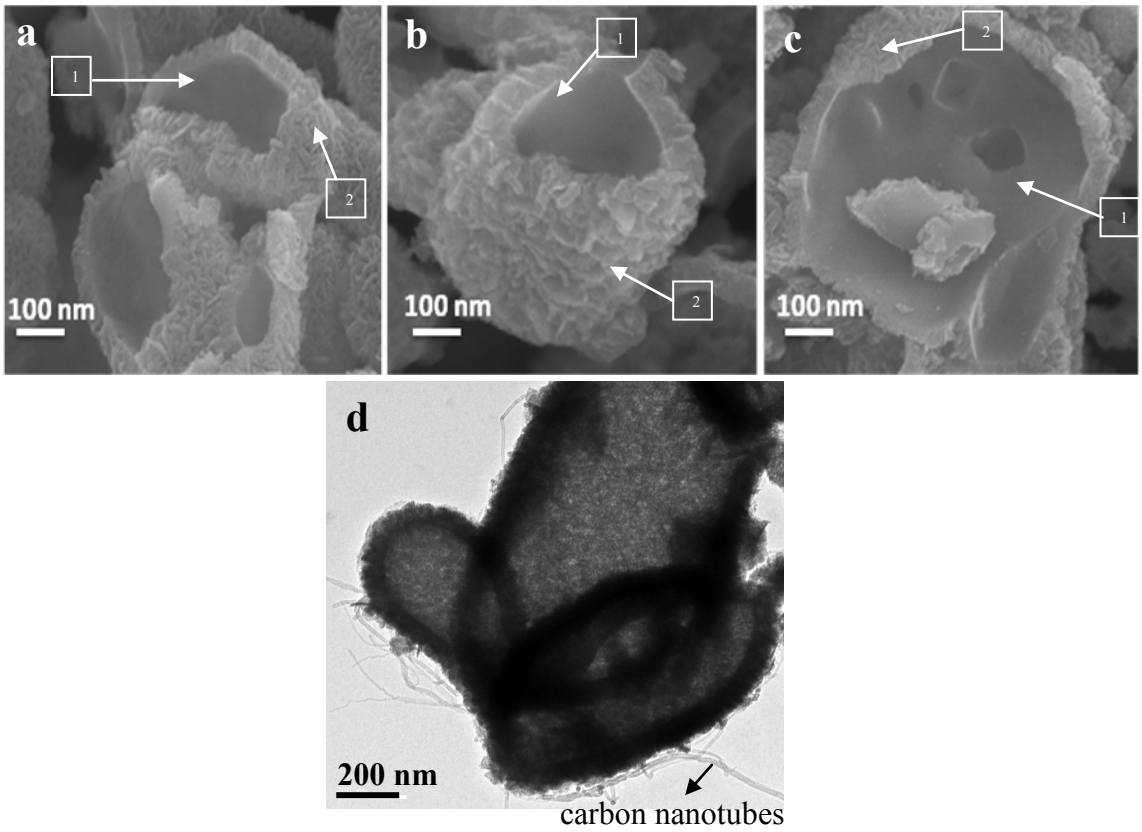

Fig. S6. (a,b,c) High magnified FE-SEM images of the hollow particles of sample C4: 1- flat surface of inner wall, 2 - roughly defined outer region. (d) TEM image of the hollow particles interconnected with carbon nanotubes (sample CC4).

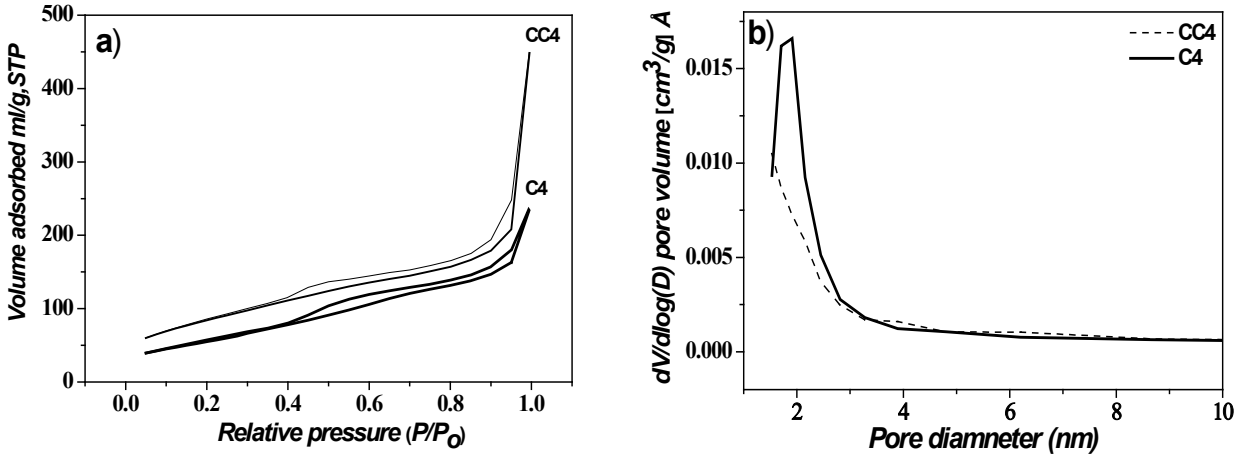

Fig. S7. (a) N_2 adsorption–desorption isotherms and (b) pore size distribution curves of samples C4 and CC4.

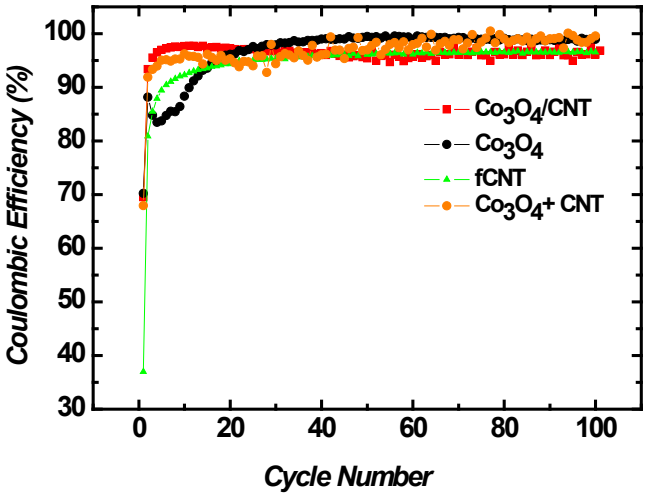

Fig. S8. Coulombic efficiencies of the Co_3O_4/CNT, Co_3O_4, Co_3O_4 + fCNT and fCNT anodes tested between 0.01-3 V (*vs* Li^+/Li) for 100 cycles at a constant current density of 50 mA g^{-1}.

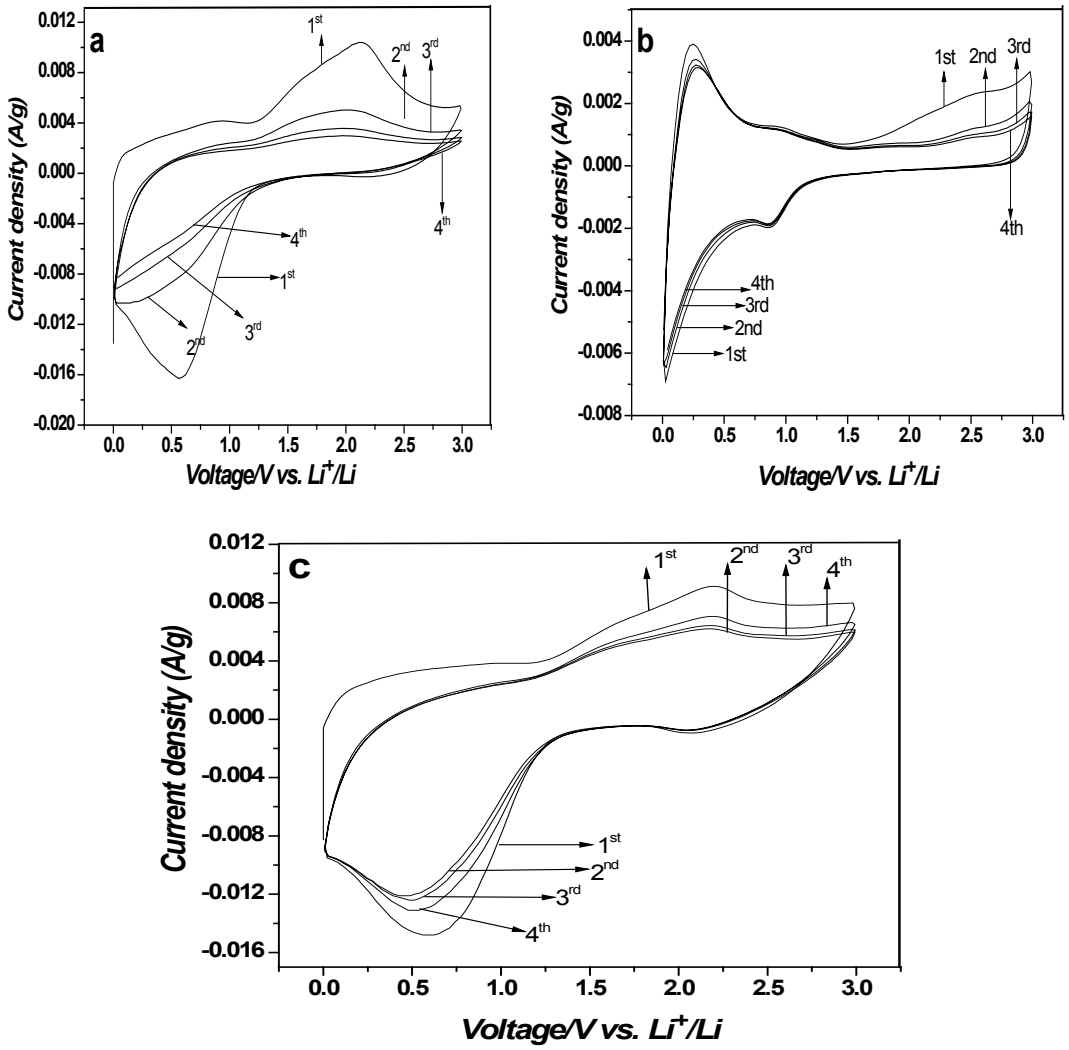

Fig. S9. Cyclic voltammograms over four cycles for (a) Co_3O_4, (b) multiwalled fCNT, and (c) Co_3O_4/CNT composite electrodes at a scanning rate of 3 mV sec^{-1} and room temperature.

We studied the electrochemical behavior of Co_3O_4, composite Co_3O_4/CNT, and fCNT electrodes by cyclic voltammetry (see Fig. S9) at a scan rate of 3 mVs^{-1}. The first cyclic voltammogram (CV) curve of Co_3O_4/CNT shows broad main reduction and oxidation peaks at around ~0.53 V and ~ 2.2 V, respectively. For Co_3O_4, a major reduction peak appears at 0.56 V with a subsequent oxidation peak at ~2.15 V. These peaks are well-correlated with the typical redox peaks corresponding to the electrochemical reaction of Co_3O_4 with Li described in the

main text.[8] The wide integral area with broad redox peaks in the initial CV curves of these samples is attributed to the expected contribution from the capacitive behavior alongside with faradaic and pseudo-capacitive processes that obviously occur for large-surface-area porous Co_3O_4 and composite Co_3O_4/CNT structures during electrochemical screening, as reported previously for other metal oxides.[12-15] Despite the broad initial CV curve, the Co_3O_4 electrode abruptly losses its characteristic curve from the second to the fourth CV cycles. For the Co_3O_4/CNT electrode, there is a sudden decrease in the integral area in the second cycle while the initial CV curve shape is maintained, and then the integral curve area increases in the third and fourth cycles. This result confirms the gain of reversible capacity due to completely reversible Li^+ redox reactions. Moreover, distinctive Li-ion intercalation and deintercalation peaks at 0 V and ~0.25 V, respectively, are seen in the CV curves of the fCNT electrodes (see Fig. S9b), as well as a reversible intense reduction peak at 0.87 V and an irreversible oxidation peak at 2.5–3 V in the first cycle.[13] During subsequent cycles, the obtained SEI layer may have contributed to the observed stable cyclability of the fCNT electrode.

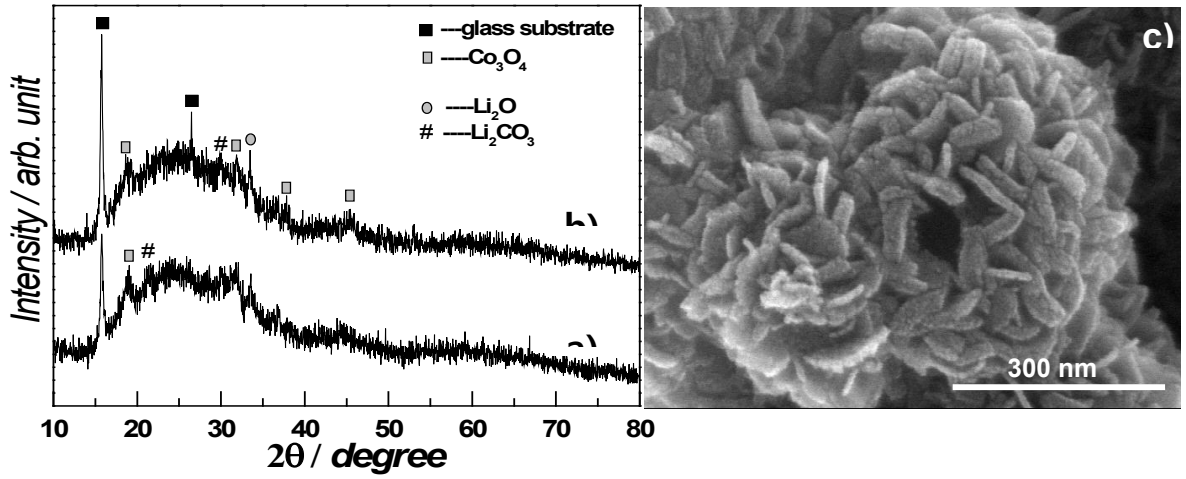

Fig. S10. XRD spectra of representative electrodes after cell testing (one charge–discharge cycle): (a) Co_3O_4 and (b) Co_3O_4/CNT; (c) SEM image of Co_3O_4/CNT electrode after ten charge-discharge cycles at 50 mA g^{-1} (25 °C).

References

1. J. Yang, H. Liu, W. N. Martens, and R. L. Frost, *J. Phys. Chem. C,* 2010, **114**, 111-119.
2. Z. P. Xu and H. C. Zeng, *Chem. Mater.,* 1999, **11**, 67-74.
3. Z. P. Xu and H. C. Zeng, *Chem. Mater.,* 2000, **12**, 3459-3465.
4. T. He, D. Chen and X. Jiao, *Chem. Mater.,* 2004, **16**, 737-743.
5. R. Xu and H. C. Zeng, *Langmuir,* 2004, **20**, 9780-9790.
6. R. Xu and H. C. Zeng, *J. Phys. Chem., B* 2003, **107**, 12643-12649.
7. T. He, D. Chen, X. Jiao, Y. Wang and Y. Duan, *Chem. Mater.,* 2005, **17**, 4023-4030.
8. Z. S. Wu, W. Ren, L. Wen, L. Gao, J. Zhao, Z. Chen, G. Zhou, Feng Li and H. M. Cheng, *ACS Nano*, 2010, **4**, 3187-3194.
9. J. Yang, H. Liu, W. N. Martens and R. L. Frost, *J. Phys. Chem. C,* 2010, **114**, 111-119.
10. T. He, D. chen, X. Jiao, Y. Wang and Y. Duan, *Chem. Mater.,* 2005, **17**, 4023-4030.
11. N. S. Melntyre and M. G. Cook, *Anal. Chem.,* 1975, **47**, 2208-2213.
12. X. M. Liu, Z. D. Huang, S. W. Oh, B. Zhang, P. C. Ma, M. M. F. Yuen and J. K. Kim, *Composites Sci. Tech*., 2012, **72**, 121-144.
13. Y. Zhang, X. Z. Zhang, H. L. Zhang, Z. G. Zhao, F. Li, C. Liu and H. M. Cheng, *Electrochim. Acta*, 2006, **51**, 4994-5000.
14. Y. M. Lin, P. R. Abel, D. W. Flaherty, J. Wu, K. J. Stevenson, A. Heller and C. B. Mullins, *J. Phys. Chem. C,* 2011, **115**, 2585-2591.

15. B. B. Owens, S. Passerini and W. H. Smyrl, *Electrochim. Acta*, 1999, **45**, 215-224.